Photosynthesis Research (2005) 84: 347–353

Regular paper

Pulse EPR, ^{55}Mn-ENDOR and ELDOR-detected NMR of the S_2-state of the oxygen evolving complex in Photosystem II

Leonid Kulik[1,2], Boris Epel[1], Johannes Messinger[1,*] & Wolfgang Lubitz[1,*]
[1]*Max Planck Institute for Bioinorganic Chemistry, 45470, Mülheim/Ruhr, Germany;* [2]*Institute of Chemical Kinetics and Combustion, Institutskaya 3, 630090 Novosibirsk, Russia; *Author for correspondence (e-mail: messinger@mpi-muelheim.mpg.de; lubitz@mpi-muelheim.mpg.de; fax: +49-208-306-3951*

Received 23 September 2004; accepted in revised form 14 February 2005

Key words: ELDOR-detected NMR, ENDOR, manganese cluster, oxygen-evolving complex, pulse EPR, S_2-state

Abstract

Pulse EPR, ^{55}Mn-ENDOR and ELDOR-detected NMR experiments were performed on the S_2-state of the oxygen-evolving complex from spinach Photosystem II. The novel technique of random acquisition in ENDOR was used to suppress heating artefacts. Our data unambiguously shows that four Mn ions have significant hyperfine coupling constants. Numerical simulation of the ^{55}Mn-ENDOR spectrum allowed the determination of the principal values of the hyperfine interaction tensors for all four Mn ions of the oxygen-evolving complex. The results of our ^{55}Mn-ENDOR experiments are in good agreement with previously published data [Peloquin JM et al. (2000) J Am Chem Soc 122: 10926–10942]. For the first time ELDOR-detected NMR was applied to the S_2-state and revealed a broad peak that can be simulated numerically with the same parameters that were used for the simulation of the ^{55}Mn-ENDOR spectrum. This provides strong independent support for the assigned hyperfine parameters.

Abbreviations: CW – continuous wave; EDTA – ethylene-diamine-tetra-acetic acid; ELDOR – electron–electron double resonance; ENDOR – electron–nuclear double resonance; EPR – electron paramagnetic resonance; ESE – electron spin echo; ESEEM – electron spin echo envelope modulation; HFI – hyperfine interaction; MLS – multiline signal; MW – microwave; NMR – nuclear magnetic resonance; NQI – nuclear quadrupole interaction; OEC – oxygen-evolving complex; PPBQ – phenyl-para-benzoquinone; PS II – Photosystem II; RF – radiofrequency

Introduction

Photosynthetic water splitting is catalyzed by the oxygen-evolving complex (OEC) of PS II, which contains a Mn_4O_xCa cluster. Despite numerous attempts, its structure is not yet fully resolved (Yachandra et al. 1993; Zouni et al. 2001; Kamiya and Shen 2003; Biesiadka et al. 2004; Ferreira et al. 2004; Messinger 2004). During the catalytic cycle (Kok cycle), the OEC passes through five different redox states, the so-called S-states (Joliot and Kok 1975). Some of these S-states (S_2, S_0) exhibit a paramagnetic ground state with a total electron spin of $S = 1/2$. The S_2-state has the strongest EPR multiline signal (MLS) and has thus been widely studied in the past by CW EPR with the aim of determining the Mn hyperfine interaction (HFI) parameters (Dismukes and Siderer 1981; Zheng and Dismukes 1996; Åhrling et al. 1998; Hasegawa et al. 1998; Lakshmi et al. 1999; Peloquin et al. 2000).

Knowledge of these parameters will provide information about the electronic structure of the OEC, which is a prerequisite for the elucidation of the mechanism of water splitting.

Unfortunately, CW EPR spectra of the OEC are extremely difficult to simulate and interpret, since the high complexity of the spin system results in a large number of fitting parameters. Thus, CW EPR data alone do not provide reliable hyperfine interaction constants for the individual Mn ions. The number of fitting parameters can be largely reduced by measuring ^{55}Mn-ENDOR of the S_2-state. Recently, Peloquin et al. (2000) reported simulations of CW EPR and ^{55}Mn-ENDOR spectra of the S_2-state using a single set of principal *g*-values and Mn HFI parameters. However, thus far no other laboratory was able to reproduce these data. It has been discussed whether (i) low sensitivity prevents the detection of ENDOR signals at high frequencies (250–400 MHz) or (ii) the spectra are affected by artefacts.

We therefore reinvestigated this question employing the advanced technique of random acquisition ENDOR, which suppresses heating artefacts (Epel et al. 2003). In addition, we employ a novel method, ELDOR-detected NMR, to obtain independent information about the Mn HFI parameters of the OEC (Schosseler et al. 1994; Mino and Ono 2003). In the version of the method used here, the two-pulse echo is created by the microwave pulse with a fixed frequency ν_1. The pulse with the variable frequency ν_2 is used to excite the forbidden electron–nuclear transitions. While ν_2 is scanned, the intensity of the echo is recorded as a function of the frequency difference $\Delta\nu = \nu_1 - \nu_2$. A peak in this ELDOR-detected NMR spectrum appears when $\Delta\nu$ is equal to the frequency of the nuclear spin transition. Thus, ELDOR-detected NMR is complementary to ENDOR. The difference to ENDOR is that the ELDOR-detected NMR spectrum usually has a stronger intensity, but a substantially larger linewidth. This comes from the fact that the excitation bandwidth of the microwave pulse is normally much larger than that of the radio frequency pulse. Thus, ELDOR-detected NMR is not the method of choice for studying small HFI constants (protons, deuterons, nitrogens). However, large HFI constants, which are often met in metal ions of enzymes, can be easily accessed by this technique. Previously, this method was applied to study partly reconstituted Mn-depleted PS II samples (Mino and Ono 2003). In this work, it is applied for the first time to functional PS II in the S_2-state. The results provide additional confirmation for Mn HFI parameters derived from ^{55}Mn-ENDOR of the S_2-state.

Materials and methods

Sample preparation

Photosystem II membranes were prepared using Triton X-100 according to (Berthold et al. 1981) and then washed three times to minimize the starch content. For storage, the preparations were resuspended to a chlorophyll concentration of about 6 mg/ml in a sucrose buffer (0.4 M sucrose, 15 mM NaCl, 5 mM $MgCl_2$, 5 mM $CaCl_2$, 50 mM Mes, pH 6.0), frozen as droplets in liquid N_2 and kept at −70 °C until use. The samples were then thawed in the dark on ice and supplemented with 1 mM EDTA, 250 μM phenyl-*p*-benzoquinone (PPBQ) and 3% methanol. Five-hundred microlitres of this suspension was transferred into each 4 mm X-band EPR tube. Then the EPR tubes were centrifuged at 4 °C for 1 h at about 6000*g* in home built adapters. This led to an approximately 3-fold concentration of the sample. The supernatant was removed in dim green light and the samples were frozen in liquid N_2. Shortly before the EPR experiments, the samples were advanced to the S_2-state by a 10 min illumination in an ethanol/dry ice bath using two 250 W halogen lamps from which the IR and UV contributions were largely removed by the following filters: 8 cm water, 2 cm $CuSO_4$ (250 mM), Schott GG 455 (2 mm) and Schott KG 3 (2 mm). The final light intensity at sample level was ~0.5 W/cm^2.

EPR measurements

Pulse EPR experiments were performed on a Bruker ESP-380E spectrometer equipped with a dielectric ring resonator. The temperature was controlled by an Oxford ITC liquid helium flow system. In all experiments, the temperature was 4.2 K. The microwave frequency ν_1 was 9.71 GHz. The length of $\pi/2$ and π pulses was 16 and 32 ns, respectively, and the delay τ between $\pi/2$ and π pulses 200 ns. The echo was integrated with a time

window of 80 ns. The shot repetition rate was 1 ms in the two-pulse echo-detected EPR experiments and 3 ms in the ^{55}Mn-ENDOR and ELDOR-detected NMR experiments.

In the ^{55}Mn-ENDOR experiments, the Davies-ENDOR pulse sequence was used with a delay between the first and the second pulse of $T = 10$ μs (see scheme in Figure 2). The length of the radiofrequency pulse was 5 μs. It was synthesized by an Agilent 4420 generator and amplified by an ENI 5100L amplifier with 100 W output power. The recently introduced random acquisition technique was used for the ^{55}Mn-ENDOR measurement (Epel et al. 2003). In such experiment, the RF is not swept sequentially, but is randomly varied in the desired range. Since in this case, the history of each point acquisition is always different, the RF-induced heat effect is averaged over the whole spectral range. This in turn decreases heating artefacts, which otherwise can manifest themselves as strong distortions of the ENDOR spectra.

For the ELDOR-detected NMR experiments, a signal generator from Rode & Schwarz, SMR40, was used as a low-power CW source for the microwave frequency ν_2. Its output was fed into the second microwave channel of the Bruker microwave bridge where it was gated and then amplified by a traveling wave tube with 1 kW output power. The length of the ν_2 microwave pulse was 9 μs. The ENDOR and ELDOR-detected NMR experiments were performed using the 'SpecMan' software (Epel et al. 2003).

In all experiments, both the illuminated (S_2) and the dark (S_1) samples were measured. Then the light-minus-dark spectrum was calculated to obtain a pure S_2-state spectrum, if the dark spectrum had non-zero intensity.

Results and discussion

Pulse EPR

Figure 1 shows the echo-detected EPR spectra for the 200 K illuminated (a, 'S_2-state'), dark-adapted (b, S_1-state) and their difference (c, pure S_2-state signal) of spinach PS II membranes containing 3% methanol. It is seen that the intensity of ESE in the dark sample is significant. Most probably it comes from cytochrome b_{559} and Cu (Astashkin et al. 1997; Mino et al. 2000; Evans et al. 2004). The intense line at 350 mT belongs to the tyrosine radical $Y_D^{\bullet}$. The light minus dark difference spectrum is approximately 170 mT wide and represents the pure S_2-state two-pulse ESE-spectrum. In its low-field part step-like features with separations of about 8.5 mT can be seen, which are characteristic for the S_2-state MLS of the OEC and thereby confirm this assignment. The absence of the step-like features in the high-field part of the spectrum may be due to (i) an insufficiently high signal-to-noise ratio or (ii) nuclear ESEEM, which is known to distort the echo-detected EPR spectrum. The arrow indicates the position in the spectrum ($B_0 = 360$ mT) where all ENDOR and ELDOR-detected NMR experiments were performed. This position was selected, because it has the highest intensity of the S_2-state ESE signal and relatively low contributions of the dark ESE signal.

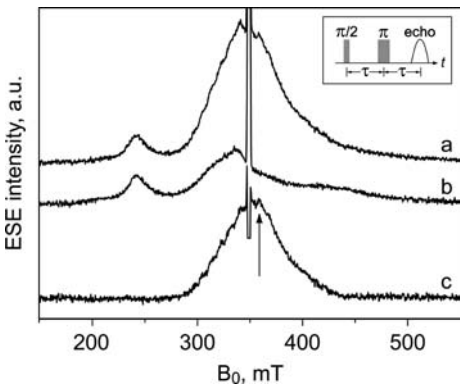

Figure 1. Echo-detected EPR spectra of the PS II membranes containing 3% methanol: (a) 200 K illuminated sample; (b) dark sample; (c) light-minus-dark difference (pure S_2-state spectrum). Microwave frequency $\nu_1 = 9.71$ GHz, $\tau = 200$ ns, temperature 4.2 K. The arrow indicates the spectral position $B_0 = 360$ mT) where all ENDOR and ELDOR-detected NMR experiments were performed. The microwave pulse sequence used in the echo-detected EPR experiment is given in the insert.

^{55}Mn-ENDOR

Figure 2 shows the dependence of the ^{55}Mn-ENDOR amplitude of the illuminated sample on the length of the RF pulse (Rabi nutations) at a radiofrequency $\nu_{RF} = 120$ MHz. This amplitude is proportional to the fraction of the nuclear spins inverted by the RF pulse. The dark sample showed no ENDOR effect in the Rabi nutation experiment (data not shown). The shape of the curve in

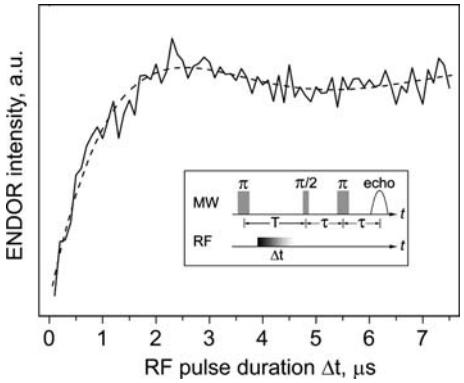

Figure 2. Rabi nutation curve (dependence of the ENDOR signal intensity on the duration of the RF pulse) for the illuminated PS II sample (S_2-state), taken at B_0 = 360 mT and ν_{RF} = 120 MHz. The dashed line is drawn to guide the eye. The Davies-ENDOR pulse sequence used is shown in the insert.

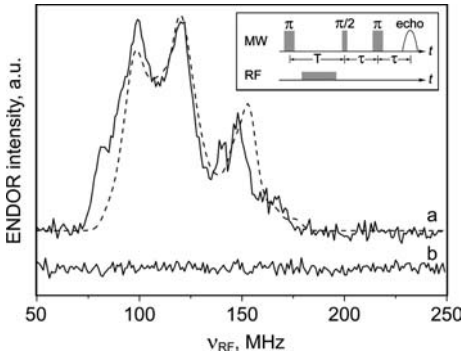

Figure 3. ^{55}Mn-ENDOR spectrum of the PS II membranes containing 3% methanol: (a) 200 K illuminated sample (S_2-state); (b) dark sample. ν_1 = 9.71 GHz, B_0 = 360 mT, τ = 200 ns, T = 10 μs, RF pulse duration Δt = 5 μs, temperature 4.2 K. The numerical simulation of the S_2-state ^{55}Mn-ENDOR spectrum with the parameters listed in Table 1 is given as dashed line. The Davies-ENDOR pulse sequence used is shown in the insert.

Figure 2 is characteristic for the ENDOR effect: the initial rise is followed by a low-amplitude oscillation. This confirms that the observed signal is caused by the nutation of the nuclear spin of Mn ions. The position of the maximum (approximately 3 μs) corresponds to the duration of the RF π-pulse. It should be noted, however, that this position was different for other RF values, which reflects the frequency dependence of the effective magnetic field B_{eff}, experienced by the nuclear spin during the RF pulse. This value depends on many factors, the most important one is the strength of the RF magnetic field B_2. It is determined by the geometry of the resonator and of the RF coils. Its influence on the ENDOR signal will be discussed below.

In Figure 3, the solid lines show the ^{55}Mn-ENDOR spectra for the illuminated sample (a, S_2-state) and for the dark sample (b, S_1-state). No features are seen in the dark spectrum. This suggests that the species producing the dark ESE spectrum does not contain nuclei with large HFI constants, or that they produce a very small ENDOR effect. A remarkably flat baseline was achieved in our ^{55}Mn-ENDOR experiments, as compared with the previous measurements (Peloquin et al. 2000). This is a result of the random acquisition in ENDOR. It is important to note that no spectral features were present in the high-frequency region (250–400 MHz) for both the S_2 and the S_1 samples (data not shown). The spectrum of the illuminated sample shows three maxima in the range between 75 and 175 MHz. The overall shape is very similar to the ^{55}Mn-ENDOR spectrum of the S_2-state measured earlier by the Britt laboratory (Peloquin et al. 2000). The main differences are (i) an improved S/N ratio due to the better baseline and (ii) some variations of the relative intensities of the three peaks. It should be noted that Rabi nutation measurements at different positions of the ENDOR spectrum show that the apparent splitting of the third peak in our spectrum (dip at 143 MHz) is of instrumental origin. It corresponds to a slowing of the initial rise in the Rabi nutation pattern, from which an about 2-fold decrease of the RF magnetic field at 143 MHz can be estimated, as compared with the 'normal level' at 138 and 148 MHz. We are currently improving the experimental setup to avoid this 'quasi-resonance' feature.

For the simulation of the obtained S_2-state ^{55}Mn-ENDOR spectrum, it is important to know how many Mn nuclei contribute to this signal. Although it is clear that the OEC contains four Mn ions, the precise structure of the Mn_4O_xCa cluster is unknown and therefore the number N of magnetically coupled Mn nuclei constituting the S_2-state EPR MLS may lie between two and four. This important question can be answered by a simple calculation using the properties of EPR and ^{55}Mn-ENDOR spectra of the OEC. First, it should be noted that due to the absence of significant orientation selectivity the mean ^{55}Mn-ENDOR frequency approximately equals one half of the

absolute value of the isotropic Mn HFI constant, averaged over all Mn nuclei, $<|A|>/2$. Using this good approximation (tests with models give results of less than 1% error), we determine from the experimental ^{55}Mn-ENDOR spectrum that $<|A|> = 235$ MHz. If we assume that the Mn HFI tensors are nearly isotropic, the contribution of Mn HFI to the width of the EPR spectrum is $W_{HFI} = 5N<|A|>$, where N is the number of Mn nuclei and the factor 5 results from the nuclear spin of the Mn ions, $I = 5/2$. Any anisotropy of Mn HFI would lead to a slight increase of W_{HFI}. We can now compare the total width of the experimental S_2-state EPR spectrum, which is $W_T = 4760$ MHz in frequency units (the width of the EPR spectrum in mT is multiplied by the electron gyromagnetic ratio, $g = 2$ is assumed), with the calculated width assuming various numbers of Mn nuclei N. With $N = 4$, a spectral width of $W_{HFI} = 4700$ MHz is calculated. The difference between W_{HFI} and W_T can be explained by a g-tensor anisotropy of $\Delta g \approx 0.02$. Due to the approximate character of this calculation, the precision of this value should not be overestimated. However, this calculation allows to safely reject the possibility of $N = 2$, since this would imply unrealistically large Δg values or different sources for the broadening of the EPR spectrum, which are not expected. The same arguments exclude $N = 3$.

The dashed line in Figure 3 shows the numerical simulation of the ^{55}Mn-ENDOR spectrum of the S_2-state with $N = 4$. This simulation is based on second-order perturbation theory. To reduce the number of fitting parameters axial g-, HFI- and NQI-tensors were used with the symmetry axis coinciding for all tensors. Furthermore, a gaussian linewidth of 4 MHz was used. The parameter set of our simulation (Table 1) coincides with that used in the previous work for the methanol-treated S_2-state (Peloquin et al. 2000), because no clear indications exist to change these values. It should be noted, however, that variations of the Mn HFI values within a range of approximately 10 MHz result in almost the same degree of visual coincidence between the experimental and the simulated spectra, because the changes can be largely compensated for by changes in the NQI parameters, which may even change sign. Thus we conclude that in contrast to the Mn HFI parameters at present the precision of the Mn NQI parameters for the S_2-state is low, and only the order of their magnitude is reliable. A further improvement of these parameters can be obtained by ^{55}Mn-ENDOR measurements at different frequencies such as Q-band.

Table 1. Parameters used in the simulation of ^{55}Mn-ENDOR and ELDOR-detected NMR spectra of the S_2-state of PS II, in MHz

^{55}Mn nucleus	$A_\perp$	$A_\parallel$	$P_\parallel$
Mn_A	−232	−270	−3
Mn_B	200	250	−3
Mn_C	−311	−270	8
Mn_D	180	240	1

$A_\perp$ and $A_\parallel$ are the principal values of the Mn HFI in perpendicular and parallel direction, respectively, and $P_\parallel$ is the major Mn quadrupole coupling parameter. The principal values $g_\perp = 1.97$ and $g_\parallel = 1.99$ were used for the g-tensor. The gaussian linewidth is 4 MHz for ENDOR and 25 MHz for ELDOR-detected NMR.

ELDOR-detected NMR

Figure 4 shows the ELDOR-detected NMR spectra for the illuminated sample (a), dark sample (b) and their difference (c). The dark spectrum (S_1-state) has a small but non-zero intensity. Its negative amplitude is probably due to a signal from species with high electron spin ($S > 1/2$) that can produce negative ESE intensity. The low-frequency peak ($\Delta\nu < 70$ MHz) in the light-minus-dark difference spectrum (c) is caused by the excitation of the allowed transitions by the ν_2 pulse. The broad peak with the maximum at 110 MHz represents the ^{55}Mn-ELDOR-detected NMR signal from the S_2-state. The different shape compared to the ^{55}Mn-ENDOR spectrum in Figure 3 is mainly due to the increased linewidth. The dashed line in Figure 4 shows the numerical simulation of the ELDOR-detected NMR spectrum. It is calculated using the same method and parameters as for the ^{55}Mn-ENDOR spectrum (Table 1). As explained earlier, the only exception to this is the linewidth, which is 25 MHz in the case of ELDOR-detected NMR compared to 4 MHz in ENDOR. Due to this rather large linewidth ELDOR-detected NMR alone can hardly be used for extraction of the individual HFI and NQI parameters of the four Mn nuclei. However, the rather good agreement of the experimental and

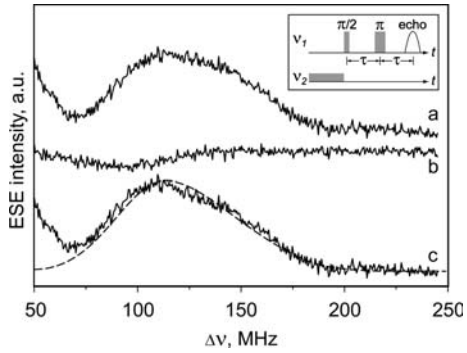

Figure 4. ELDOR-detected NMR spectra of the PS II membranes containing 3% methanol: (a) 200 K illuminated sample; (b) dark sample; (c) light-minus-dark difference (pure S_2-state spectrum). The numerical simulation of the S_2-state ^{55}Mn-ELDOR-detected NMR spectrum with the parameters listed in Table 1 is given as dashed line. The ELDOR-detected NMR pulse sequence is given in the insert.

theoretical spectra in Figure 4 provides additional support for the parameter set derived from ^{55}Mn-ENDOR.

Conclusions

The pulse EPR and ^{55}Mn-ENDOR spectra of the OEC in the S_2-state presented in this paper confirm previously published data by the Britt laboratory (Peloquin et al. 2000). This is important, since their derived effective hyperfine parameters differ significantly from all previously published once (Zheng and Dismukes 1996; Åhrling et al. 1998; Hasegawa et al. 1998). Our new data add additional trust to these HFI parameters, because the new method of random acquisition was employed to collect the ^{55}Mn-ENDOR data in order to suppress heating artefacts. As a consequence, a remarkably flat baseline was obtained for the S_1 control sample over the entire frequency range, which makes a subtraction procedure for the S_2-state unnecessary. A careful analysis of Rabi nutations also ensures that true ENDOR signals are observed.

For the first time also ELDOR-detected NMR spectra of the S_2-state are presented. These data strongly support the HFI parameters derived from the X-band ^{55}Mn-ENDOR experiments, because an excellent agreement between the experimental data and a simulation using the ENDOR derived parameter set is obtained. Additional support comes from our recent ^{55}Mn-ENDOR spectra, recorded at a different microwave frequency (Q-band), which can be simulated well with very similar HFI parameters, but somewhat different NQI parameters (Kulik et al. 2005).

The ultimate goal of these experiments is to derive the electronic and geometric structure of the OEC. For this, the effective HFI parameters need to be deconvoluted into the intrinsic HFI parameters. This work is beyond the scope of this present communication but will be completed in due course. At present, we are not able to further comment on possible structures of the OEC or the oxidation states of the four Mn ions in the S_2-state. However, on the basis of (i) simple considerations (vide supra) and (ii) the absence of any ENDOR signals in the range between 200 and 400 MHz, we can already safely exclude all models proposing two magnetically uncoupled dimers as structural elements of the OEC in the S_2-state.

Acknowledgements

The authors are grateful to K.O. Schäfer and R. Bittl who were involved in the initial stages of ^{55}Mn-ENDOR experiments. LVK is thankful to the Alexander von Humboldt foundation for the financial support. This work was supported by DFG, Grant Me 1629/2-3, by Sfb 498 (TP C5) and by the Max Planck Society.

References

Åhrling KA, Smith PJ and Pace RJ (1998) Nature of the Mn centers in Photosystem II. Modeling and behavior of the $g = 4$ resonances and related signals. J Am Chem Soc 120: 13202–13214

Astashkin AV, Mino H, Kawamori A and Ono T-A (1997) Pulsed EPR study of the S′$_3$ signal in the Ca^{2+}-depleted Photosystem II. Chem Phys Lett 272: 506–516

Berthold DA, Babcock GT and Yocum CF (1981) A highly resolved, oxygen-evolving Photosystem II preparation from spinach thylakoid membranes. FEBS Lett 134: 231–234

Biesiadka J, Loll B, Kern J, Irrgang KD and Zouni A (2004) Crystal structure of cyanobacterial Photosystem II at 3.2 angström resolution: a closer look at the Mn-cluster. Phys Chem Chem Phys 6: 4733–4736

Dismukes GC and Siderer Y (1981) Intermediates of a polynuclear manganese cluster involved in photosynthetic oxidation of water. Proc Natl Acad Sci USA 78: 274–278

Epel B, Arieli D, Baute D and Goldfarb D (2003) Improving W-band pulsed ENDOR sensitivity-random acquisition and pulsed special TRIPLE. J Magn Reson 164: 78–83

Evans MCW, Nugent JHA, Ball RJ, Muhiuddin I and Pace RJ (2004) Evidence for a direct manganese-oxygen ligand in water binding to the S_2 state of the photosynthetic water oxidation complex. Biochemistry 43: 989–994

Ferreira KN, Iverson TM, Maghlaoui K, Barber J and Iwata S (2004) Architecture of the photosynthetic oxygen-evolving center. Science 303: 1831–1838

Hasegawa K, Kusunoki M, Inoue Y and Ono T-A (1998) Simulation of S_2-state multiline EPR signal in oriented Photosystem II membranes: structural implications for the manganese cluster in an oxygen-evolving complex. Biochemistry 37: 9457–9465

Joliot P and Kok B (1975). Oxygen evolution in photosynthesis. In: Govindjee (ed) Bioenergetics of Photosynthesis, pp 387–412. Academic Press, New York

Kamiya N and Shen J-R (2003) Crystal structure of oxygen-evolving photosystem II from *Thermosynechococcus vulcanus* at 3.7 Å resolution. Proc Natl Acad Sci USA 100: 98–103

Kulik LV, Epel B, Lubitz W and Messinger J (2005) ^{55}Mn pulse ENDOR at 34 GHz of the S_0 and S_2 states of the oxygen-evolving complex in Photosystem II. J Am Chem Soc 127: 2392–2393

Lakshmi KV, Eaton SS, Eaton GR and Brudvig GW (1999) Orientation of the tetranuclear manganese cluster and tyrosine Z in the O_2-evolving complex of Photosystem II: an EPR study of the $S_2Y_Z^{\bullet}$ state in oriented acetate-inhibited Photosystem II membranes. Biochemistry 38: 12758–12767

Messinger J (2004) Evaluation of different mechanistic proposals for water oxidation in photosynthesis on the basis of Mn_4O_xCa structures for the catalytic site and spectroscopic data. Phys Chem Chem Phys 6: 4764–4771

Mino H and Ono T (2003) Applications of pulsed ELDOR-detected NMR measurements to studies of Photosystem II: magnetic characterization of Y_D tyrosine radical and Mn^{2+} bound to the high-affinity site. Appl Magn Reson 23: 571–583

Mino H, Kawamori A and Ono T (2000) Pulsed EPR studies of doublet signal and singlet-like signal in oriented Ca^{2+}-depleted PS II membranes: location of the doublet signal center in PS II. Biochemistry 39: 11034–11040

Peloquin JM, Campbell KA, Randall DW, Evanchik MA, Pecoraro VL, Armstrong WH and Britt RD (2000) ^{55}Mn ENDOR of the S_2-state multiline EPR signal of Photosystem II: implications on the structure of the tetranuclear Mn cluster. J Am Chem Soc 122: 10926–10942

Schosseler P, Wacker T and Schweiger A (1994) Pulsed ELDOR detected NMR. Chem Phys Lett 224: 319–324

Yachandra VK, DeRose VJ, Latimer MJ, Mukerji I, Sauer K and Klein MP (1993) Where plants make oxygen: a structural model for the photosynthetic oxygen evolving manganese cluster. Science 260: 675–679

Zheng M and Dismukes GC (1996) Orbital configuration of the valence electrons, ligand field symmetry, and manganese oxidation states of the photosynthetic water oxidizing complex: analysis of the S_2 state multiline EPR signals. Inorg Chem 35: 3307–3319

Zouni A, Witt HT, Kern J, Fromme P, Krauß N, Saenger W and Orth P (2001) Crystal Structure of Photosystem II from *Synechococcus elongatus* at 3.8 Å resolution. Nature 409: 739–743